

Accurate Measurement of Normal Vectors of the Heart from MRI Data Using Variational Calculus

T. Rachidi, L. Coghlan, and A. Amar
Al-Akhawayn University in Ifrane
PO.BOX 104, Ifrane, 53 000
Morocco
{rachidi,L.Coghlan}@alakhawayn.ma

Abstract

Normal vectors are of primary importance in reconstructing the surface of the left ventricle from MR images of the heart. They are fundamental for accurate measurement of wall thickness, which is a very important parameter in assessing ventricular function. In this work, we present a novel technique for computing accurate normal vectors. This technique is based on variational calculus. It explicitly enforces and controls the smoothness of normal vectors along and across outlines. The computed normal vectors are used to describe the surface of the LV through the fit of local osculating paraboloids. Principal curvatures and principal directions are also computed. Besides being fast and simple, this approach applies equally well to the right ventricle, and more generally to any surface sampled in terms of digitized outlines. Extensive experiments are performed using simulated surfaces, for varying sampling resolution to determine the robustness and accuracy of the suggested method. Finally, this method is applied to segmented MR images of the human left ventricle, and the results are presented.

1 Introduction

This research is part of a project whose primary goal is the development of a precise method for assessing ventricular function and myocardial viability [4, 6, 7, 9, 10, 11, 12, 13] based on the evaluation of ventricular geometry, from data obtained from magnetic resonance images. Precise functional assessment is crucial in defining which patients are operable and likely to benefit from cardiac surgery (valvular repair, revascularisation, ...), thereby guiding decisions that are critical to patient outcomes. It is also fundamental for determining the right moment for surgical referral without allowing a deterioration of function that can jeopardize the result of surgical treatment.

In assessing ventricular function from geometry, accurate information about wall thickness and principal curvatures [9] are essential. Precise knowledge of normal vectors, in particular, allows measurement of principal curvatures and principal directions. This gives very detailed assessment of the local *in vivo* (differential) geometry of the heart, which allows, in particular, more accurate measurement of *wall thickness* than presently used “in plane” methods. The latter do not take into account the inclination of the image plane to the wall. This is especially a problem near the apex of the left ventricle [7, 13]. Furthermore, knowledge of wall thickness and principal curvatures is essential in quantifying remodeling of the left ventricle due to valvular disease and following myocardial infarction. The goal of our work is to compute accurate normal vectors and principal curvatures of the left ventricle walls, from data in the form of digitised short axis MRI images.

2 Previous work

In order to reconstruct the surface of the left ventricle (LV), three main techniques have been proposed in the literature:

1. Model-based techniques, which try to approximate the shape of LV using simple analytical objects like spheres, ellipsoids, or cylinders [16, 19, 21]. The latter have been found to offer only a coarse approximation, due to their oversimplified geometry. More elaborate 3-D surface models have been proposed. Bending and stretching models [17], axisymmetrical models [18], and deformable models [20, 14] are examples of such techniques. The main limitation with these techniques is that they are better suited for estimating the motion of the wall, rather than measuring parameters such as principal curvatures and principal directions, and wall thickness.

2. Surface-based techniques that compute directly the parametrisation of the wall surfaces from segmented data [8]. Polynomials are generally used to approximate surfaces. Curvature measures are functions of the partial derivatives of the approximating polynoms.

3. Normal vectors-based techniques that first compute normal vectors, and then deduce the local parametrisation of the surface [4, 5]. In [4], the normal vectors, together with the directions of principal curvature, are computed from the osculating paraboloid that locally approximates data from outlines. The osculating paraboloid is estimated using Newton’s method to refine an initial estimate. A major drawback of this technique is its inability to correctly approximate principal curvature in the orthogonal direction to the outlines, because equal importance is given to points from neighboring stacks. A further limitation with this technique is its inefficiency. Indeed, the osculating paraboloid is computed for each iteration of the Newton’s method. Moreover, it has been shown in [15] that, the cross product method used to approximate initial normal vectors is by far not the best, and thus Newton’s scheme may not converge on the right normal vector. Furthermore, there is no local coherence, *i.e.*, neighbouring normal vectors may not vary smoothly along and across outlines.

To overcome the above mentioned problems, we have developed a novel technique for computing accurate and coherent normal vectors of the LV from segmented MR images: A robust and accurate initial approximation of normal vectors [15], is followed by an iterative scheme for refining initial normal vectors, while enforcing the smoothness constraint across and along outlines. The degree of smoothness is explicitly controlled. Points lying on the same outline contribute more to the smoothing than points from neighbouring outlines. Extensive experiments are performed using simulated ellipsoids, elliptic paraboloids, and hyperboloids of one sheet. The differences (in angles) between the computed and the theoretical normals are used to evaluate this technique. These experiments are carried out for various sampling resolutions in order to determine the robustness and accuracy of the suggested method. The results are compared to [4]. Finally, this method is applied to segmented MR images of the human left ventricle, and the results are presented.

3 Our approach

Assume a global **X-Y-Z** coordinate system and a set of outlines, resulting from the segmentation of MR

images of the heart as in **Fig. 1**. Each outline O_i is a set of point triplets $P_i(x, y, z)$. Let $P \in O_i$ be a point of interest at which we wish to compute the normal vector \vec{n} .

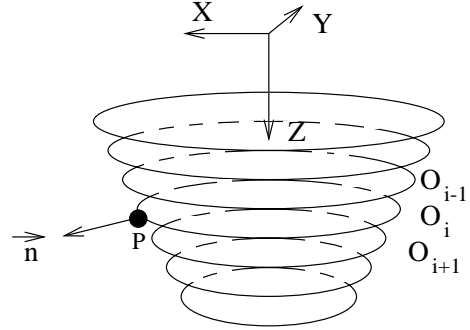


Fig. 1. A set of artificial outlines $\{\dots O_{i-1}, O_i, O_{i+1} \dots\}$ representing segmented MR images of the left ventricle. $P \in O_i$ is the point of interest. \vec{n} is the normal vector to the surface at P .

3.1 Surface normals

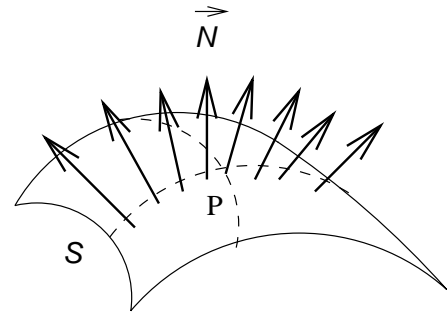


Fig. 2. A unit normal vector field \vec{N} to the surface S .

Let S be a surface, and \vec{N} be a unit normal vector field to S . It can be easily shown that if S is smooth, then locally at a point P , S is of the form $F(x, y, z) = 0$ where $F(x, y, z)$ is a C^∞ function, and that $\vec{N}(\vec{P})$ (\vec{N} at P) is either $\frac{\nabla F}{\|\nabla F\|}$, or $-\frac{\nabla F}{\|\nabla F\|}$. It follows that the unit normal vector field \vec{N} is smooth.

Locally, near P , the surface S can also be parameterized as $S(u, v) = (X(u, v), Y(u, v), Z(u, v))$. Then \vec{N} is given by:

$$\vec{N} = \frac{\frac{\partial S}{\partial u} \times \frac{\partial S}{\partial v}}{\|\frac{\partial S}{\partial u} \times \frac{\partial S}{\partial v}\|} \quad (1)$$

We denote the components of \vec{N} by $p(u, v)$, $q(u, v)$, and $r(u, v)$.

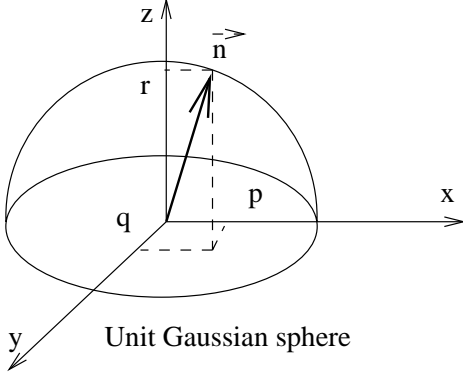


Fig. 3. The Gaussian sphere illustrating the components of the vector \vec{N} at point P : $\vec{N}(P) = \vec{n}$.

Equation (1) expresses the fact that the cross product of the velocity vectors along any two curves on the surface S and passing through a point P , is collinear to the normal $\vec{N}(P)$ to S at P . For fixed curves C_1 and C_2 , let \vec{t}_1 and \vec{t}_2 be the velocity vectors of C_1 and C_2 at P . Let $\vec{n} = \vec{N}(P)$, then equation (1) can be rewritten as:

$$\|\vec{n} - \frac{\vec{t}_1 \times \vec{t}_2}{\|\vec{t}_1 \times \vec{t}_2\|}\|^2 = 0 \quad (2)$$

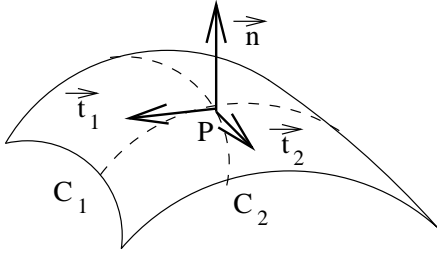


Fig. 4. \vec{t}_1 , and \vec{t}_2 are the tangent vectors to the curves C_1 and C_2 at P .

Writing $\vec{n} = (p, q, r)^t$, where $p^2 + q^2 + r^2 = 1$; equation (2) can be rewritten as follows:

$$(p - a)^2 + (q - b)^2 + (r - c)^2 = 0 \quad (3)$$

where a, b , and c are computed from the tangents \vec{t}_1 and \vec{t}_2 at P to the curves C_1 and C_2 . For our purpose, C_1 is taken to be the outline O_i to which P belongs, and C_2 is taken to be the circle that goes through point P and its two closest points from neighboring outlines O_{i-1} and O_{i+1} . Note that this curve does not necessarily lie on the surface. However, it is expected

to be a good approximation, especially if the inter-outline distance α is small.

If we define a function $R(p, q, r) = 1 - ap - bq - cr$, then (3) yields:

$$R(p(u, v), q(u, v), r(u, v)) = 0 \quad (4)$$

3.2 Smoothness constraint

We assume that the left ventricle is made up of piecewise smooth surfaces which depart from the smoothness assumption only along sets of small measure. Let P be a point of interest, and $\vec{n} = (p, q, r)^t$ the normal vector to the left ventricle surface at P (see Fig. 1). From Section 3.1, a smooth surface is characterized by continuously varying normals, or similarly the gradients of p, q and r being small. Thus if p_u, p_v, q_u, q_v, r_u , and r_v represent the partial derivatives of p, q and r , we can specify the smoothness constraint as minimizing the integral of the sum of the squares of these partial derivatives as follows:

$$e_s = \int \int [(p_u^2 + p_v^2) + (q_u^2 + q_v^2) + (r_u^2 + r_v^2)] dudv \quad (5)$$

This integral must be minimized subject to the constraint given in (4). However, to account for noise, the problem is posed as that of minimizing total error e given by

$$e = e_s + \lambda e_t \quad (6)$$

where λ is a control parameter which weighs the error in smoothness constraint relative to the error in the surface tangents equation given by

$$e_t = \int \int R^2(p, q, r) dudv \quad (7)$$

3.3 The algorithm

Minimizing the error in (6) is a well known problem in variational calculus applied to computer vision [2], and the solution of which is the following iterative scheme for updating the value of (p, q, r) :

$$p_{ij}^{(n+1)} = p_{ij}^{(n)} + \lambda R(p_{ij}^{*(n)}, q_{ij}^{*(n)}, r_{ij}^{*(n)}) \frac{\partial R}{\partial p} \quad (8)$$

$$q_{ij}^{(n+1)} = q_{ij}^{(n)} + \lambda R(p_{ij}^{*(n)}, q_{ij}^{*(n)}, r_{ij}^{*(n)}) \frac{\partial R}{\partial q} \quad (9)$$

$$r_{ij}^{(n+1)} = r_{ij}^{(n)} + \lambda R(p_{ij}^{*(n)}, q_{ij}^{*(n)}, r_{ij}^{*(n)}) \frac{\partial R}{\partial r} \quad (10)$$

where $*$ denotes the average values computed in a $m \times m$ neighborhood, and the subscripts i, j denote discrete positions near the point P .

3.4 Choice of averaging neighborhood

To further control smoothness along and across outlines, a weighted average is adopted. Formally, let $P_{ij} \in O_i$, be the point of interest, and let O_{i-1} and O_{i+1} be the two neighboring outlines to O_i (see **Fig. 5**). Let also $(P_{kh})_{k \in \{i-1, i, i+1\}; h \in \{j-1, j, j+1\}}$ be the 3×3 closest points to P_{ij} from the three outlines O_{i-1}, O_i , and O_{i+1} . The averaged expressions $p_{ij}^{*(n)}$, $q_{ij}^{*(n)}$, and $r_{ij}^{*(n)}$ are computed as follows:

$$p_{ij}^{*(n)} = \sum_{\substack{k \in \{i-1, i, i+1\} \\ h \in \{j-1, j, j+1\}}} w_{kh} p_{kh}^{(n)} \quad (11)$$

$$q_{ij}^{*(n)} = \sum_{\substack{k \in \{i-1, i, i+1\} \\ h \in \{j-1, j, j+1\}}} w_{kh} q_{kh}^{(n)} \quad (12)$$

$$r_{ij}^{*(n)} = \sum_{\substack{k \in \{i-1, i, i+1\} \\ h \in \{j-1, j, j+1\}}} w_{kh} r_{kh}^{(n)} \quad (13)$$

where

$$w_{kh} = \begin{bmatrix} \frac{1}{16} & \frac{1}{8} & \frac{1}{16} \\ \frac{1}{8} & \frac{1}{4} & \frac{1}{8} \\ \frac{1}{16} & \frac{1}{8} & \frac{1}{16} \end{bmatrix}$$

These weights are used so that closer points to the point of interest have higher weights, and thus contribute more to the smoothing. However, if the inter-slice gap α is small enough, (see **Fig. 5**), these weights can be changed to reflect confidence in points from outlines O_{i-1} and O_{i+1} .

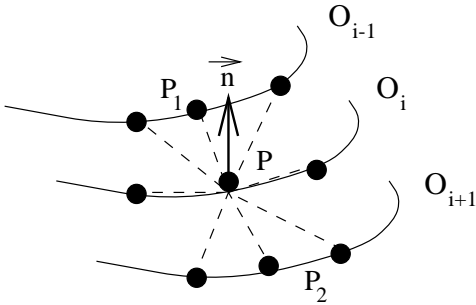


Fig. 5. The 3×3 closest points to P used to compute the weighted average. α is the inter-slice thickness.

3.5 Computing surface geometry

Using the normal vectors computed in **Section 3.3**, the steps for computing the main curvature features (or equivalently surface geometry), namely the principal curvature directions and their corresponding principal curvatures are as follows:

1. construct a local orthogonal coordinate system $\vec{x} - \vec{y} - \vec{n}$ where \vec{n} is the normal to the surface at the point P under focus.
2. translate the points in the neighborhood of P from the global original coordinate system to the new coordinate system.
3. compute the parameters of the osculating paraboloid (14) at P . This is posed as finding the parameters of the paraboloid (14) that best fits the set of neighboring points, in a least square sense.

$$z = Ax^2 + By^2 + 2Cxy + Dx + Ey + G \quad (14)$$

The principal curvatures at a point P are given by:

$$k_1 = A + B + \sqrt{(A - B)^2 + 4C^2} \quad (15)$$

and

$$k_2 = A + B - \sqrt{(A - B)^2 + 4C^2} \quad (16)$$

and the principal directions by the normalization of the vectors:

$$\vec{f}_1 = \frac{2C}{k_1 - 2A} \vec{i} + \vec{j}, \quad (17)$$

and

$$\vec{f}_2 = \frac{2C}{k_2 - 2A} \vec{i} + \vec{j} \quad (18)$$

where \vec{i} and \vec{j} are the unit vectors along the positive \vec{x} and \vec{y} directions; A , B , and C are parameters of the osculating paraboloid (14)

4 Evaluation of the technique

Ellipsoids (19), elliptic paraboloids (20), and hyperboloids (21) of one sheet are used to test the this technique.

$$\frac{x^2}{a^2} + \frac{y^2}{b^2} + \frac{z^2}{c^2} = 1 \quad (19)$$

$$z = ax^2 + by^2 \quad a > 0, b > 0 \quad (20)$$

$$\frac{x^2}{a^2} + \frac{y^2}{b^2} - \frac{z^2}{c^2} = 1 \quad (21)$$

These shapes are used because they provide good test cases for positive and negative Gaussian curvatures. Zero Gaussian curvature is of little relevance

for this study. Outlines are constructed by sampling points from these surfaces at various inter-slice thickness α .

For various values of α , average, minimum and maximum angle differences (in degrees) between computed and theoretical normals, together with standard deviations are computed. Furthermore, the average percentage difference (22) between principal curvatures of the osculating paraboloids and the theoretical principal curvatures (computed from (19) to (21)), together with standard deviations, are computed.

$$\%D_{avg} = \frac{\sqrt{(k_1 - k_{1th})^2 + (k_2 - k_{2th})^2}}{\sqrt{k_{1th}^2 + k_{2th}^2}} \times 100 \quad (22)$$

5 Results

For the first set of experiments, the CPM method [15] has been used to compute initial normals. The parameter λ which weighs the error in smoothness constraint relative to the error in the surface tangents has been fixed to $\lambda = 0.001$. For each surface type, three main results are presented, namely:

1. a table summarizing the results obtained for computing normals using our technique (VCM). These results are compared to the CM method from [15].
2. a graph illustrating the convergence of VCM.
3. a table summarizing the results obtained after computing curvatures for various neighborhood sizes N .

Table 1 summarizes the results obtained for the ellipsoids ($a = b = 30, 40$ and 50 mm, and $c = 90$ mm). The total average error in the angle, E_{avg} (in degrees), and the standard deviation σ are computed over all outlines of the ellipsoids.

| α | 9 mm | | 10 mm | | 12 mm | |
|----------|-----------|----------|-----------|----------|-----------|----------|
| | E_{avg} | σ | E_{avg} | σ | E_{avg} | σ |
| CM | 0.17 | 0.22 | 0.21 | 0.26 | 0.25 | 0.30 |
| VCM | 0.00 | 0.00 | 0.00 | 0.00 | 0.00 | 0.00 |

Table 1. Total average error E_{avg} and standard deviations σ in degrees for the Circles Method (CM) and the Variational Calculus Method (VCM), on ellipsoids ($a = b = 30, 40, 50$ mm and $c = 90$ mm), for different inter-slice thicknesses α .

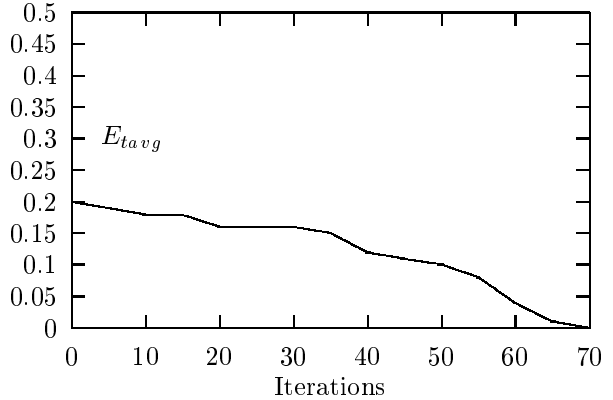


Fig. 6. Variation of the average error (in degrees) as a function of the number of iterations, for the elliptic paraboloid $a = b = 30$ mm and $c = 90$ mm, for an inter-slice thickness $\alpha = 10$ mm, and $\lambda = 0.01$. As the number of iteration increases, the total average error E_{avg} steadily decreases until it reaches zero.

Table 2 summarizes the results obtained for the ellipsoids ($a = b = 30, 40$ and 50 mm, and $c = 90$ mm) and different neighborhood sizes N . The total average percentage difference, $\%D_{avg}$, and the standard deviation σ are computed over all outlines of the ellipsoids.

| α | 9 mm | | 10 mm | | 12 mm | |
|----------|-------------|----------|-------------|----------|-------------|----------|
| | $\%D_{avg}$ | σ | $\%D_{avg}$ | σ | $\%D_{avg}$ | σ |
| 9 | 1.07 | 0.20 | 1.17 | 0.33 | 1.47 | 0.92 |
| 15 | 0.72 | 0.12 | 1.00 | 0.31 | 1.22 | 0.43 |
| 21 | 1.86 | 1.05 | 1.96 | 0.89 | 2.01 | 1.13 |

Table 2. Total average percentage difference $\%D_{avg}$ and standard deviations σ , on the ellipsoids ($a = b = 30, 40, 50$ mm and $c = 90$ mm), for different inter-slice thicknesses α , and different neighborhood size N .

Fig. 7 displays the normal vectors obtained by VCM for the ellipsoid ($a = b = 40$ mm and $c = 60$ mm).

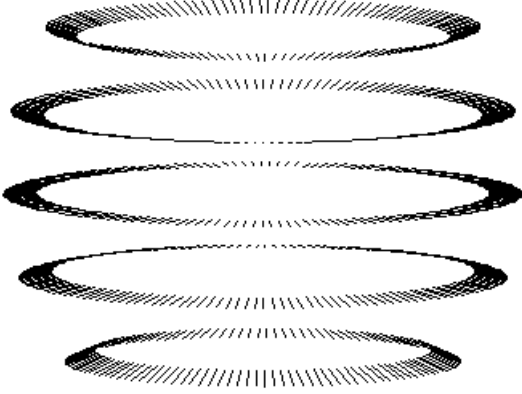


Fig. 7. Normal vectors obtained by VCM for the ellipsoid ($a = b = 40$ mm and $c = 60$ mm).

Table 3 summarizes the results obtained for the elliptic paraboloids ($a = b = 0.2, 0.3$ and 0.4 mm). The total average error in the angle, E_{tavg} (in degrees), and the standard deviation σ are computed over all outlines of the elliptic paraboloids.

| α | 9 mm | | 10 mm | | 12 mm | |
|----------|------------|----------|------------|----------|------------|----------|
| | E_{tavg} | σ | E_{tavg} | σ | E_{tavg} | σ |
| CM | 0.14 | 0.17 | 0.15 | 0.19 | 0.16 | 0.22 |
| VCM | 0.00 | 0.00 | 0.00 | 0.00 | 0.00 | 0.00 |

Table 3. Total average error E_{tavg} and standard deviations σ in degrees for the Circles Method (CM) and the Variational Calculus Method (VCM), on the elliptic paraboloids ($a = b = 0.2, 0.3, 0.4$ mm), for different inter-slice thicknesses α .

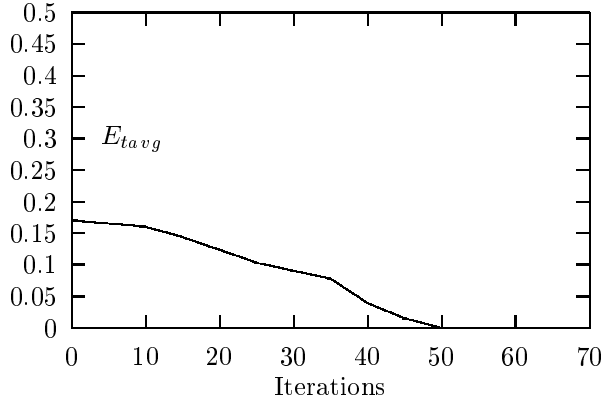


Fig. 8. Variation of the average error (in degrees) as a function of the number of iterations, for the elliptic paraboloid $a = b = 0.3$ mm, for an inter-slice thickness $\alpha = 10$ mm, and $\lambda = 0.01$. As the number of iteration increases, the total average error E_{tavg} steadily decreases until it reaches zero.

Table 4 summarizes the results obtained for the elliptic paraboloids ($a = b = 0.2, 0.3$ and 0.4 mm) and different neighborhood size N . The total average percentage difference, $\%D_{tavg}$, and the standard deviation σ are computed over all outlines of the ellipsoids.

| α | 9 mm | | 10 mm | | 12 mm | |
|----------|--------------|----------|--------------|----------|--------------|----------|
| | $\%D_{tavg}$ | σ | $\%D_{tavg}$ | σ | $\%D_{tavg}$ | σ |
| 9 | 0.97 | 0.11 | 1.02 | 0.20 | 1.31 | 0.42 |
| 15 | 0.61 | 0.08 | 0.73 | 0.31 | 0.96 | 0.39 |
| 21 | 1.02 | 0.31 | 1.12 | 0.51 | 1.47 | 0.88 |

Table 4. Total average percentage difference $\%D_{tavg}$ and standard deviations σ , on the elliptic paraboloids ($a = b = 0.2, 0.3, 0.4$ mm), for different inter-slice thicknesses α , and different neighborhood size N .

Fig. 9 displays the normal vectors obtained by VCM for an elliptic paraboloid.

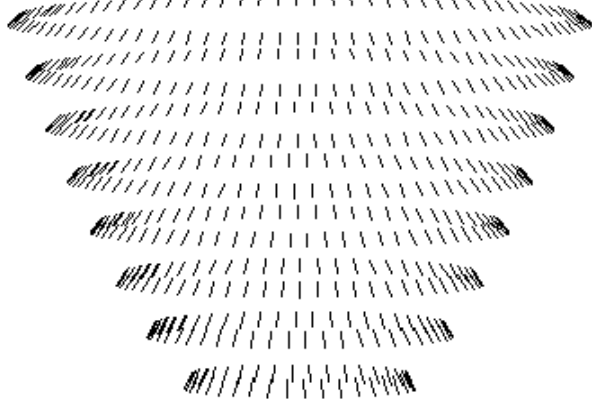


Fig. 9. Normal vectors obtained by VCM for the elliptic paraboloid ($a = b = 0.2$ mm).

Table 5 summarizes the results obtained for the hyperboloids of one sheet ($a = b = 30, 40$ and 50 mm, and $c = 90$ mm). The total average error in the angle, E_{tavg} (in degrees), and the standard deviation σ are computed over all outlines of the hyperboloids of one sheet.

| α | 9 mm | | 10 mm | | 12 mm | |
|----------|------------|----------|------------|----------|------------|----------|
| | E_{tavg} | σ | E_{tavg} | σ | E_{tavg} | σ |
| CM | 0.06 | 0.05 | 0.07 | 0.05 | 0.08 | 0.06 |
| VCM | 0.01 | 0.00 | 0.01 | 0.00 | 0.01 | 0.00 |

Table 5. Total average error E_{tavg} and standard deviations σ in degrees for the Circles Method (CM) and the Variational Calculus Method (VCM), on the hyperboloids of one sheet ($a = b = 30, 40, 50$ mm and $c = 90$ mm), for different inter-slice thicknesses α .

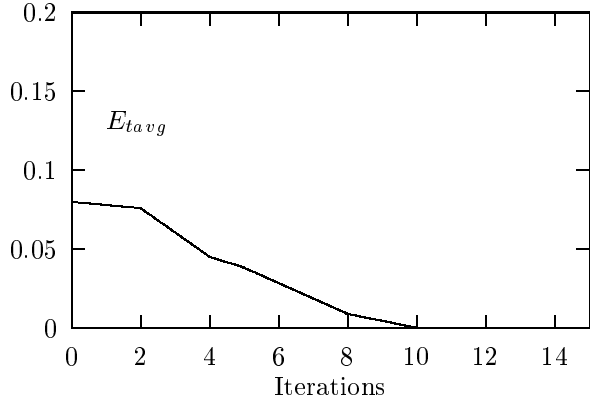


Fig. 10. Variation of the average error (in degrees) as a function of the number of iterations, for the hyperboloids of one sheet ($a = b = 30$ mm and $c = 90$ mm), for an inter-slice thickness $\alpha = 10$ mm, and $\lambda = 0.01$. As the number of iteration increases, the total average error E_{tavg} rapidly decreases until it reaches zero.

Table 6 summarizes the results obtained for the hyperboloids of one sheet ($a = b = 30, 40, 50$ mm and $c = 90$ mm) and different neighborhood size N . The total average percentage difference, $\%D_{tavg}$, and the standard deviation σ are computed over all outlines of the ellipsoids.

| α | 9 mm | | 10 mm | | 12 mm | |
|----------|--------------|----------|--------------|----------|--------------|----------|
| | $\%D_{tavg}$ | σ | $\%D_{tavg}$ | σ | $\%D_{tavg}$ | σ |
| 9 | 0.82 | 0.21 | 0.99 | 0.71 | 1.07 | 0.62 |
| 15 | 0.79 | 0.32 | 0.81 | 0.70 | 1.00 | 0.27 |
| 21 | 1.13 | 0.87 | 1.32 | 0.81 | 1.58 | 0.43 |

Table 6. Total average percentage difference $\%D_{tavg}$ and standard deviations σ , on the hyperboloids of one sheet ($a = b = 30, 40, 50$ mm and $c = 90$ mm), for different inter-slice thicknesses α , and different neighborhood size N .

Fig. 11 displays the normal vectors obtained by VCM for a hyperboloid of one sheet.

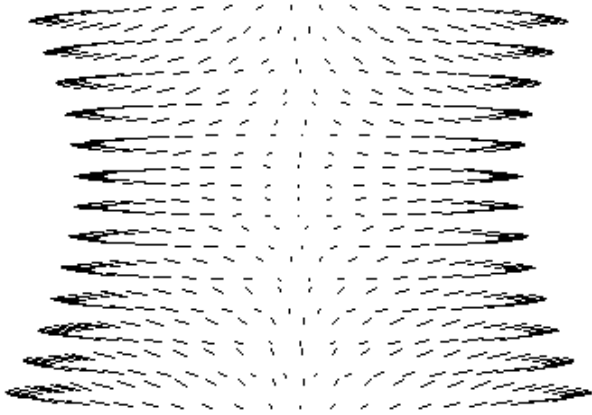


Fig. 11. Normal vectors obtained by VCM for the hyperboloid of one sheet ($a = b = 40$ mm and $c = 60$ mm).

6 Discussion

The first set of results shows that for plausible inter-slice thicknesses ($\alpha \leq 12$ mm), the proposed method outperforms CM. It computes normal vectors accurately up to a precision of 1/100 th. for all types of curvatures. Moreover, the iterative scheme upon which this technique is built converges rapidly (at most 4 mn on a shared Sparc 1000 server). Moreover, principal direction curvatures are computed with an error $\%D_{avg} \in [0.61..1.86] \pm 1.12$ for interslice-thicknesses $\alpha \leq 12$ mm. As expected, this error decreases for smaller interslice-thicknesses. As far as size of the neighborhood used for computing curvature information is concerned, it appears that $N = 15$ is the optimal value for all interslice thicknesses. Larger values would cause far away points to affect the accuracy of the computations. Smaller values would mean that not enough information is provided for computing the osculating paraboloid model.

6.1 Real data from segmented heart MRI

Fig. 12 shows the normal vectors gotten for the real heart outlines of Fig. 13.

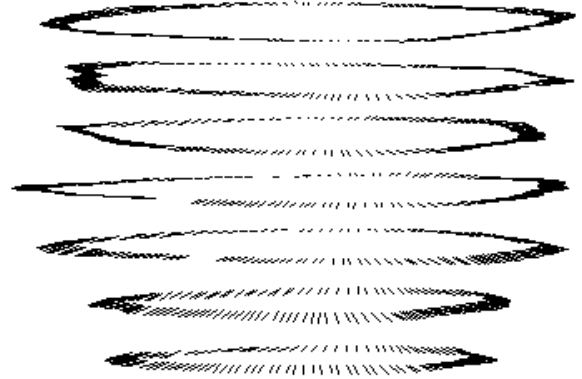


Fig. 12. Normal vectors obtained by VCM for the outlines in Fig. 13.

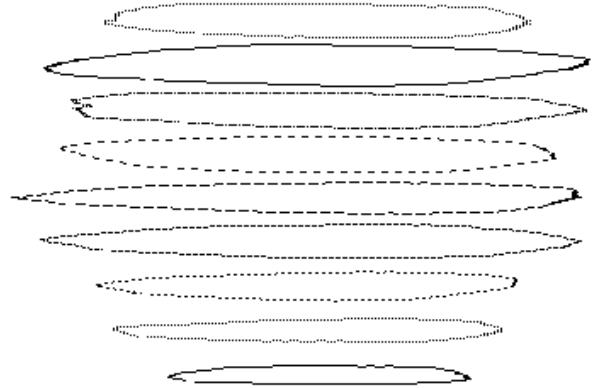


Fig. 13. Manually segmented data of a real heart.

7 Conclusions

Enforcing smoothness along and across outlines allows us to improve the results of previous techniques for computing initial normals. The Variational Calculus Method (VCM) presented in this paper gives perfect results when tested with known geometrical shapes.

The VCM algorithm runs fast with a time complexity of $O(n \times I)$ where n is the number of points in all slices and I is the total number of iterations.

8 Acknowledgements

The authors would like to thank The University of Alabama for providing cardiac MR images.

References

- [1] M. Brady and A. Yuille. *An extremum principle for shape from contour*. IEEE Trans. Pattern Anal. Mach. Intell., vol. PAMI-6, pp. 288-301, 1984.
- [2] K. Ikeuchi and B. K. P. Horn. *Numerical shape from shading and occluding boundaries*. Artif. Intell., vol. 19, pp. 141-185, 1981.
- [3] A. P. Wilkin. *Recovering surface shape and orientation from texture*. Artif. Intell., vol. 17, pp. 17-47, 1981.
- [4] L. Coghlan, H. R. Singleton, L. J. Dell'Italia, C. E. Linderholm, G. M. Pohost. *Measurement of three dimensional normal vectors, principal curvatures, and wall thickness of the heart using cine-MRI*. SPIE Medical Imaging, San Diego, CA, SPIE, Vol. 2433, pp. 292-302, 1995.
- [5] L. Coghlan, H. R. Singleton, C. E. Linderholm, G. M. Pohost. *Measurement of normal vectors, principal curvatures, and wall thickness using cine-MRI*. Submitted to PAMI.
- [6] L. J. Dell'Italia, L. Coghlan, H. R. Singleton, G. G. Bladewell, G. M. Pohost. *Curvature-wall Thickness product by magnetic resonance imaging: an index of myocardial adaptation to load*. Society of Magnetic Resonance in Medicine. 12th Annual meeting, August, 14-20, New York, N. Y. 1993.
- [7] M. A. Lawson, L. L. Johnson, L. Coghlan, H. R. Singleton, E. L. Tauxe, G. M. Pohost. *End-systolic wall thickness in the assessment of myocardial viability*. International Society of Magnetic Resonance in Medicine. 4th Annual meeting, April 27-May 3, New York, N. Y. 1996.
- [8] E. M. Stokely and S. Y. Wu. *Surface parametrization and curvature measurement of arbitrary 3-D objects: 5 practical methods*. IEEE Trans. Pattern Anal. Mach. Intell., vol. PAMI-8, pp. 833-840, 1992.
- [9] J. Lessick, S. Sideman, H. Azhari, E. Shapiro, J. L. Weiss, and R. Beyar. *Evaluation of regional load in acute ischemia by three-dimensional curvatures analysis of the left ventricle*. Ann. Biomed. Eng. Vol. 21, pp. 147-161, 1993.
- [10] R. C. Semelka, E. Tomei, S. Wagner, J. Mayo, C. Kondo, J. I. Suzuki, G. R. Caputo, and C. B. Higgins. *Normal left ventricular dimensions and function: interstudy reproducibility of measurements with cine-MR imaging*. Radiology 174:763-768, 1990.
- [11] M. C. Dulce, G. H. Mostbeck, K. K. Frieze, G. R. Caputo, and C. B. Higgins. *Quantification of the left ventricular volumes and function with cine-MR imaging: comparison of geometric models with three-dimensional data*. Radiology 188:371-376, 1993.
- [12] M. S. Sacks, C. J. Chuong, G. H. Templeton, and R. Peshock. *"In vivo" 3-D reconstruction and geometric characterization of the right ventricular free wall*. Ann. Biomed. Eng., Vol. 21, pp. 263-275, 1993.
- [13] M. A. Lawson, L. L. Johnson, L. Coghlan, M. Alami, E. L. Tauxe, S. S. Reinert, H. R. Singleton, and G. M. Pohost. *Correlation of Thallium Uptake with Left Ventricular Wall Thickness by Cine MRI in Patients with Myocardial Infarctions*. Amer. Journ. Cardiology. Vol. 80 pp. 434-441. 1997.
- [14] J. Park, D. Metaxas, A. A. Young, and L. Axel. *Deformable Models with Parameter Functions for Cardiac Motion Analysis from Tagged MRI Data*. IEEE Trans. on Medical Imaging. Vol. 15 No. 3. pp. 278-289, 1996.
- [15] A. Amar, T. Rachidi, L. Coghlan, A. Bensaid, H. Benjelloun, M. Benomar, and S. Imani. *Measurement of Normal Vectors of the Left Ventricle from Segmented MRI: Comparison of four Practical Methods*. 1st MIUA, Oxford, July 1997.
- [16] T. Arts, W. C. Hunter, A. Douglas, M. M. Muijtjens, and R. S. Reneman. *Description of the Deformation of the left ventricle by a kinematic model*. J. Biomech., vol. 25 no. 10 pp. 1119-1127, 1992.
- [17] A. Amimi, J. Ducan. *Pointwise tracking of left-ventricle motion in 3-D*, in Proc. of IEEE Workshop on Visual Motion, Princeton, NJ, pp. 294-298, 1991.
- [18] E. Bardinnet, V. Ayache, and L. D. Cohen. *Fitting of iso-surfaces using superquadratics and free-form deformations*, in Proc. of IEEE Workshop on Biomedical Image Analysis, Seattle, WA, pp. 184-193, 1994.
- [19] R. Beyar, and S. Sideman. *Effect of the twisting motion on the nonuniformities of transmural fiber mechanics and energy demand*, IEEE Trans. Biomed. Eng., Vol. BME-32, pp. 764-769, 1985.
- [20] L. D. Cohen, and I. Cohen. *A finite element method applied to new active contour models and 3-D reconstruction from cross sections*, in Proc. 3rd Int. Conf. Comput. Vision, Osaka, Japan, pp. 587-591, 1990.
- [21] H. C. Kim, B. G. Min, M. M. Lee, J. D. Seo, Y. W. Lee, and M. C. Han. *Estimation of local cardiac wall deformation and regional wall stress from biplane coronary cineangiograms*, IEEE Trans. Biomed. Eng., Vol. BME-32, pp. 503-511, 1985.